Batako, A

Dynamic FEA analysis of the Super Lightweight External cryogenic fuel tank (SLWT) made of Aluminium alloy 2195 - graphene nano composite for launch vehicle aerospace application

Dynamic FEA analysis of the Super Lightweight External cryogenic fuel tank (SLWT) made of Aluminium alloy 2195 - graphene nano composite for launch vehicle aerospace application

P. Ashwath [1], Syed Saad Salman [2], M. Venkatraman [3], Alicia Patel [1,4], M. Anthony Xavior [3], Andre Batako [5,*], Jeyapandiarajan Paulsamy [3] and Joel Jayaseelan [3]

[1] Faculty of Engineering, Environment and Computing, Coventry University, United Kingdom CV1 5FB.
[2] Department of Design Engineering, Safran Seats GB, Wales, United Kingdom, NP443HQ.
[3] School of Mechanical Engineering, Vellore Institute of Technology, Vellore, Tamil Nadu, India 630014.
[4] Defence Equipment and Support, Bristol, United Kingdom, BS34 8JH.
[5] General Engineering Research Institute, LJMU, Liverpool, United Kingdom L3 5UX.
* Correspondence: a.d.batako@ljmu.ac.uk

Abstract: This research presents a comprehensive dynamic finite element analysis (FEA) of a cryogenic fuel tank made from an innovative aluminium/lithium graphene nano-composite material, assessing its suitability for aerospace launch vehicles carrying cryogenic hydrogen and oxygen. The study focuses on the effects of light-weighting, utilizing 0.5 wt.% reinforced graphene in the AL-2195 matrix, a material poised to revolutionize the aerospace industry. Objectives include developing a digital twin of the fuel tank, CAD modeling to aerospace standards, and conducting ANSYS simulations under launch conditions to evaluate stress, strain, and deformation. Numerical results reveal a significant weight reduction of approximately 19,420 kg and a notable maximum stress reduction of 1.3% compared to traditional AL-2195 alloy tanks. The novelty of this research lies in its pioneering analysis of aluminium/lithium-graphene composites for light-weighting in cryogenic fuel tanks under space launch conditions. Conclusions affirm the composite's viability, advocating for the development of lighter yet robust aerospace structures and fostering innovation in spacecraft design and materials science.

1. Introduction

As humanity embarks on ambitious missions to explore the uncharted territories of Mars and the Moon, the demand for advanced materials capable of enhancing spacecraft performance has come to the forefront of space exploration engineering. Central to this endeavour is the imperative to increase payload capacity, a pivotal factor in enabling sustained human presence beyond Earth's orbit. In response to this challenge, researchers have long relied on aluminium alloys for their exceptional combination of low density and mechanical properties, making them the backbone of space exploration engineering [1-7].

The External Tank (ET) of the Space Shuttle, a crucial component, underwent significant evolutionary changes throughout the progress of space exploration. Starting with the standard-weight tank, it progressed to the lightweight tank (LWT) and ultimately to the super lightweight tank (SLWT). The SLWT, first used on STS-91 in 1998, marked a major technological advancement. It was constructed using the 2195 aluminium-lithium alloy, which was both 40% stronger and 10% less dense than the previously used material. This change resulted in a substantial weight reduction of 3,400 kg (7,500 lb), enhancing the Shuttle's performance and payload capacity [8-13].

However, the widespread adoption of aluminium-lithium (Al-Li) alloys has been hindered by historical concerns surrounding anisotropic properties, poor toughness, and thermal stability issues. In this context, aluminium alloy 2195 (AA 2195), characterized by its composition of Al-4.0Cu-1Li-0.4Mg-0.4Ag-0.1Zr, has emerged as a third-generation alloy with significant potential for cryogenic tankage applications in space launch systems (SLS) and space transportation systems (STS). NASA's successful utilization of AA 2195 in super lightweight cryogenic tanks for space shuttles underscores its pivotal role in advancing space exploration [14]. Despite the advancements achieved with aluminium alloys, the emergence of graphene-based composite materials presents a new era of possibilities in lightweighting strategies for aerospace applications. Graphene, renowned for its exceptional strength, conductivity, and lightweight properties, serves as an effective reinforcing agent in metal matrix composites (MMCs), offering superior mechanical performance and durability [15].

In the context of cryogenic storage systems for aerospace applications, the liquid oxygen (LOX) and liquid hydrogen (LH_2) tanks are subjected to intricate physical forces and thermal conditions that must be meticulously managed to ensure optimal performance and safety in the newly considered composite material for the tanks [10-15]. Gravitational and hydrostatic forces play a crucial role in determining the behavior and distribution of the cryogenic fluids within these tanks made of novel graphene reinforced composite material. Gravitational forces affect the overall pressure exerted by the liquid column, while hydrostatic forces influence the pressure distribution at various depths, impacting the structural integrity of the tank and the stability of the stored fluids [16].

In addition to the mechanical forces, the thermal dynamics within LOX and LH_2 tanks are of vital importance. These tanks must maintain extremely low temperatures to keep the oxygen and hydrogen in their liquid states, typically around -183°C for LOX and -253°C for LH_2. The thermal management in the fuel tanks are effectively achieved by controlling heat transfer mechanisms such as conduction, convection, and radiation to minimize heat ingress from the external environment. This is often achieved through usage of efficient structural materials, advanced insulation techniques and active cooling systems to prevent vaporization and potential pressure build-up within the tanks [12-15].

The interplay between these forces and thermal dynamics necessitates a comprehensive understanding of cryogenic fluid behavior under varying conditions. Engineers must account for factors such as stratification, thermal gradients, and fluid sloshing, which can affect the performance and safety of the propulsion system [16]. Consequently, the design and operation of LOX and LH_2 tanks involve sophisticated modelling and simulation techniques to predict and mitigate potential issues, ensuring reliable and efficient storage and transfer of these critical propellants in aerospace missions [17].

Along with the thermal dynamics and forces involved on the tanks the other primary challenge was the tank's weight. Initially, the EFT was designed as a standard-weight tank, but the need to enhance the Shuttle's payload capacity led to the development of the Lightweight Tank (LWT) and subsequently the Super Lightweight Tank (SLWT). The SLWT represented a significant technological advancement, utilizing the 2195 aluminium-lithium alloy, which was both stronger and less dense than the previous materials used. The use of alternative lightweight composite materials for aerospace launch vehicle external fuel tank structural components. The focus is on developing graphene-reinforced Aluminium metal matrix composites and studying their metallurgical and mechanical properties for potential use in space exploration applications, particularly in the external fuel tank structural applications of launch vehicles [8].

Graphene, characterized by its distinctive two-dimensional arrangement of carbon atoms forming a hexagonal lattice, has revolutionized multiple scientific fields [9-12]. This material's exceptional blend of attributes, including outstanding electrical conductivity, remarkable mechanical strength, and notable flexibility, has positioned it at the forefront of research, particularly in aerospace engineering [13]. Its unique properties offer significant potential for innovation and advancement in aerospace and space exploration sector [21]. Nonlinear behaviour in aerospace structures has attracted considerable interest among researchers. When exposed to diverse loads and conditions, these structures frequently display behaviours that diverge from standard linear elastic responses [22]. Such nonlinearities may stem from the materials used, the structural geometry, or a mix of both factors. The Super Lightweight External Tank (SLWT), with its complex design and dynamic operational environment, also exhibits these nonlinear behaviours.

The Super Lightweight External Tank (SLWT) demonstrates a variety of nonlinear responses. Previous research [23-25] thoroughly explore this behaviour, which include bifurcation-type buckling, short-wavelength nonlinear bending, and nonlinear collapse. Understanding each of these responses is vital, particularly in evaluating the SLWT's functionality across different stages of a Shuttle mission. This research also highlights the necessity of identifying and managing these nonlinearities to maintain the structural integrity and safety of the SLWT by employing the composite materials properties as the tank material property [26]. Finite-element models are crucial in forecasting and comprehending the dynamic and nonlinear behaviours of the Super Lightweight External Tank (SLWT). The significance of employing high-fidelity finite-element models for precise depiction of the SLWT's reactions are found to be important. These models provide detailed insights into the SLWT's behaviours, allowing for simulations under various scenarios and the prediction of possible challenges [27].

In the pursuit of more efficient and cost-effective aerospace launch vehicles, the exploration of lightweight materials has emerged as a pivotal area of research and development. The drive towards lightweighting not only enhances payload capacity and fuel efficiency but also mitigates structural stresses during launch and operation. This imperative has led researchers to investigate alternate super lightweight materials capable of withstanding the extreme conditions of space exploration. This paper delves into the exploration of graphene-based composite materials as a means of achieving lightweighting objectives in aerospace launch vehicles. Through a comprehensive design validation process at dynamic levels, the study aims to assess the feasibility and efficacy of these materials in enhancing the performance and resilience of launch vehicle structures. By investigating the mechanical properties and structural behaviour of graphene-based composites under launch conditions, this research endeavours to contribute to the advancement of lightweighting strategies in aerospace engineering.

The subsequent sections will delve into the methodology employed for material characterization, CAD modelling conforming to aerospace standards, and dynamic finite element analysis (FEA) to evaluate the performance of graphene-based composite materials. Furthermore, the paper will discuss the implications of these findings for the future design and development of aerospace launch vehicles, emphasizing the potential for graphene composites to redefine the standards of lightweighting in space exploration.

2. Functionality of the tank components and Methodology

Figure 1 presents a structured methodology for a comparative analysis of the dynamic behaviour of a cryogenic fuel tank assembly constructed from AL 2195 and an AL 2195-Graphene composite. This study is conducted under conditions typical of aerospace operations. The approach encompasses the use of our experimental data gathered for the AL 2195-graphene composite, comprehensive modelling, simulation, and validation processes. A multi-faceted quantitative strategy is employed to reinforce the reliability and precision of the validations carried out. This method integrates numerical data derived from simulations with empirical evidence gathered from our previous technical documents and experimental studies related to the Al-2195 graphene composite and pure Al 2195 material. This technique facilitates a comprehensive statistical examination of the material characteristics and the performance of the fuel tanks in simulated scenarios.

Each component of the cryogenic fuel tank assembly (LOX tank, Intertank, and LH_2 tank) was modelled using SolidWorks 2023 as shown in figure 2. The models were constructed to exact specifications based on the design parameters obtained from the NASA technical report (Lockheed Martin Space System, 2008) and reflected the precise geometry required for FEA. The individual parts will be assembled in SolidWorks to represent the complete cryogenic fuel tank structure as it would be configured in a launch vehicle. The fuel tank assembly ensured that all parts are correctly aligned and interfaced. Before proceeding to the simulation phase, the SolidWorks model was validated by comparing it with existing designs and by conducting preliminary checks for any geometrical inconsistencies. A critical phase involved substituting the standard alloys with the innovative Al 2195-Graphene Composite material. This change was vital to examine the improved attributes offered by the composite. By transferring the model into ANSYS 2023, emphasis was placed on the quality of the mesh and the boundary conditions, replicating real-life situations such as gravitational and hydrostatic forces, along with the thermal dynamics of LOX and LH_2 with the dimensions and scale of the model mentioned in table 1.

Table 1. SLWT Specification.

SLWT Technical Specification	Full Scale Model (1:1)
Length	153.8 ft (46.9 m)
Diameter	27.6 ft (8.4 m)

The LOX tank depicted in Figures 3a, representing the Super Lightweight Fuel Tank (SLWT) in Computer-Aided Design (CAD) modelling, is positioned atop the External Tank (ET). It adopts an ogive shape aimed at minimizing aerodynamic drag and aero thermodynamic heating [28]. This ogive nose section comprises a flat removable cover plate and a nose cone, housing a detachable conical assembly that acts as an aerodynamic fairing for propulsion and electrical system components [28-31]. The leading portion of the nose cone serves as a cast aluminium lightning rod. The LOX tank's capacity is measured at 19,744 cubic feet (559.1 m3) at 22 psi (150 kPa) and −297 °F (90.4 K; −182.8 °C) (cryogenic), according to Ferrick et al. (2008). The tank feeds into a 17 in (430 mm) diameter feed line that conveys the liquid oxygen through the Intertank, then outside the ET to the aft right-hand ET/orbiter disconnect umbilical [32]. The 17 in (430 mm) diameter feed line permits liquid oxygen to flow at approximately 2,787 lb./s (75,800 kg/min) with the RS-25s operating at 104% or permits a maximum flow of 17,592 US gal/min (1.1099 m^3/s) [33-35].

Table 2. LOX Tank Technical Specification.

LOX Technical Specification	Full Scale Model (1:1)
Length	54.6 ft (16.6m)
Diameter	27.6 ft (8.4 m)
Operation Pressure	34.7 – 36.7 Psi (absolute)

The Intertank in Figure 3b is the structural connection between the LOX and LH_2 tanks of the Super lightweight (SLWT) external tank. Its primary functions include receiving and distributing all thrust loads from the Solid Rocket Boosters (SRBs) and transferring loads between the tanks. The two SRB forward attach fittings, located 180° apart on the Intertank structure, are critical for load management [36]. A beam extends across the Intertank structure and is mechanically fastened to these attach fittings. During Solid Rocket boosters (SRB) firing, this beam flexes under high stress loads, transferring these loads to the fittings (Wingate, 2012). Adjacent to the SRB attach fittings is a major ring frame. The loads from the fittings are transferred to this frame, which then distributes the tangential loads to the Intertank skin.

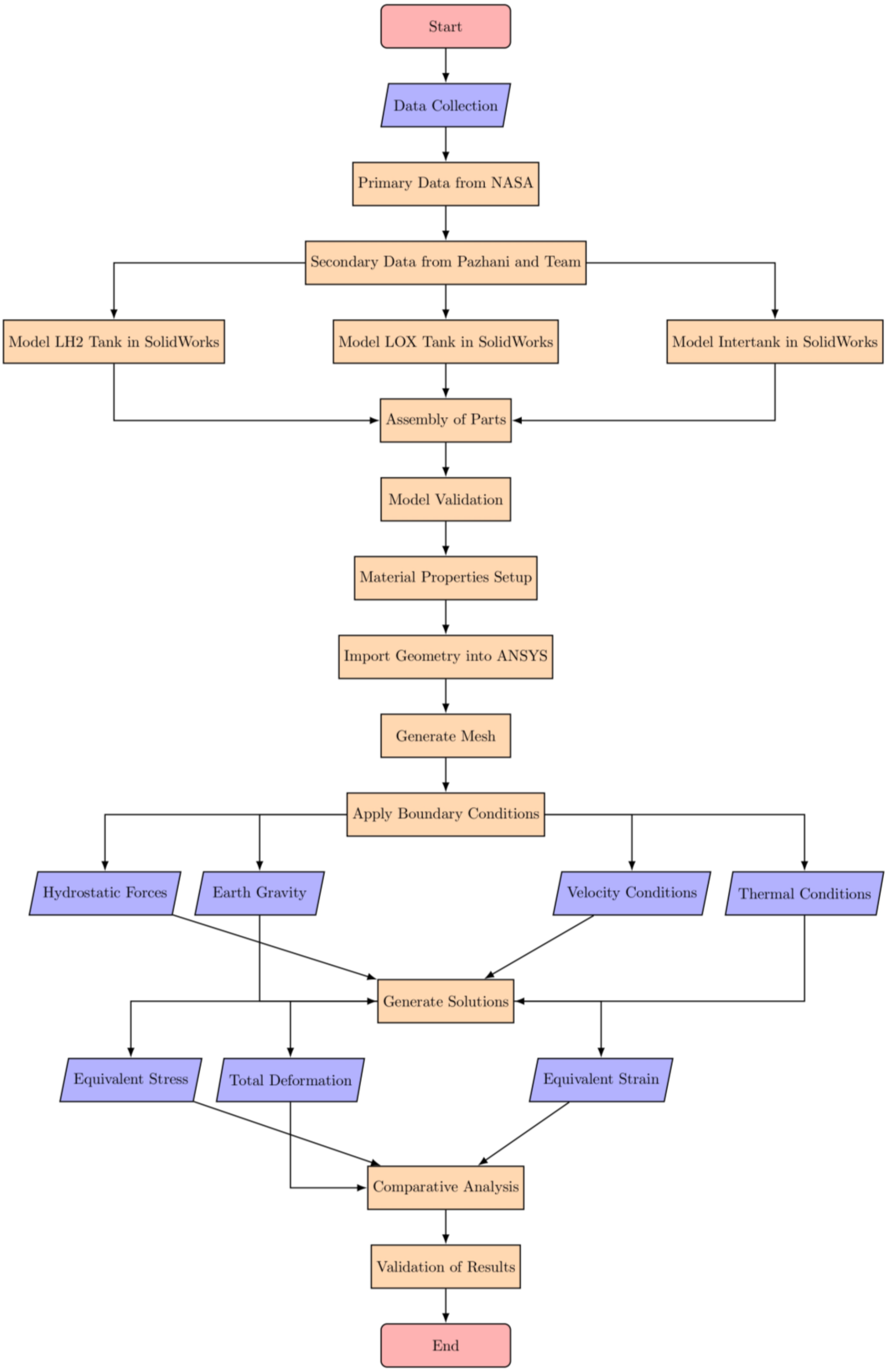

Figure 1. Process Flow Chart.

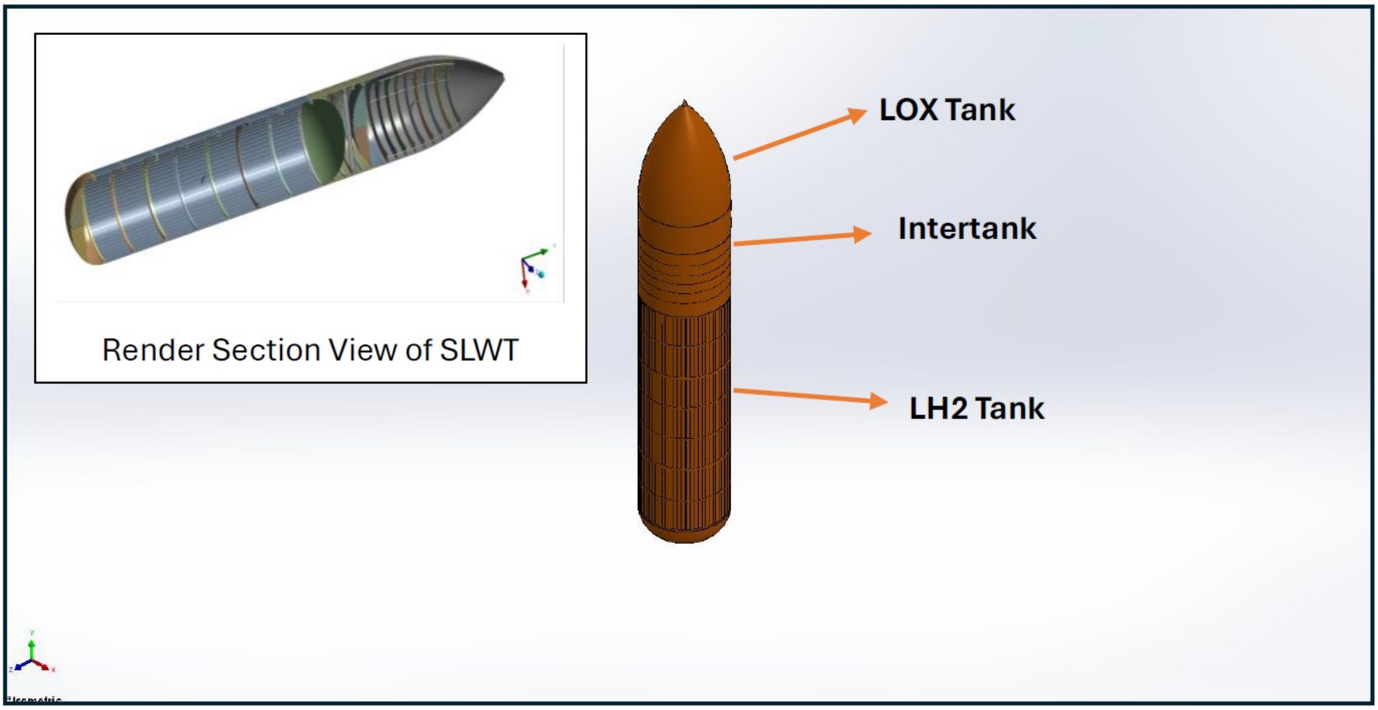

Figure 2. CAD model of SLWT of Launch Vehicle Scale 1:1.

The thrust panels of the Intertank, two panels of its skin, distribute the concentrated axial SRB thrust loads to the LOX and LH_2 tanks and to adjacent Intertank skin panels, which are made up of six stringer-stiffened panels [37-41]. These structural components are crucial for maintaining the integrity of the Intertank under the extreme conditions of space launch.

Additionally, the Intertank functions as a protective compartment for housing operational instrumentation, which is vital for the successful operation of the Space Shuttle [42]. The cryogenic moisture analysis of materials used in areas like the Intertank flange is also an essential aspect of ensuring the safety and functionality of the ET (Nasa & Asrc Aerospace Corp., 2018). Table 3 shows the Intertank Technical Specification.

Table 2. Intertank Technical Specification.

Intertank Technical Specification	Full Scale Model (1:1)
Length	22.6 ft (6.9m)
Diameter	27.6 ft (8.4 m)

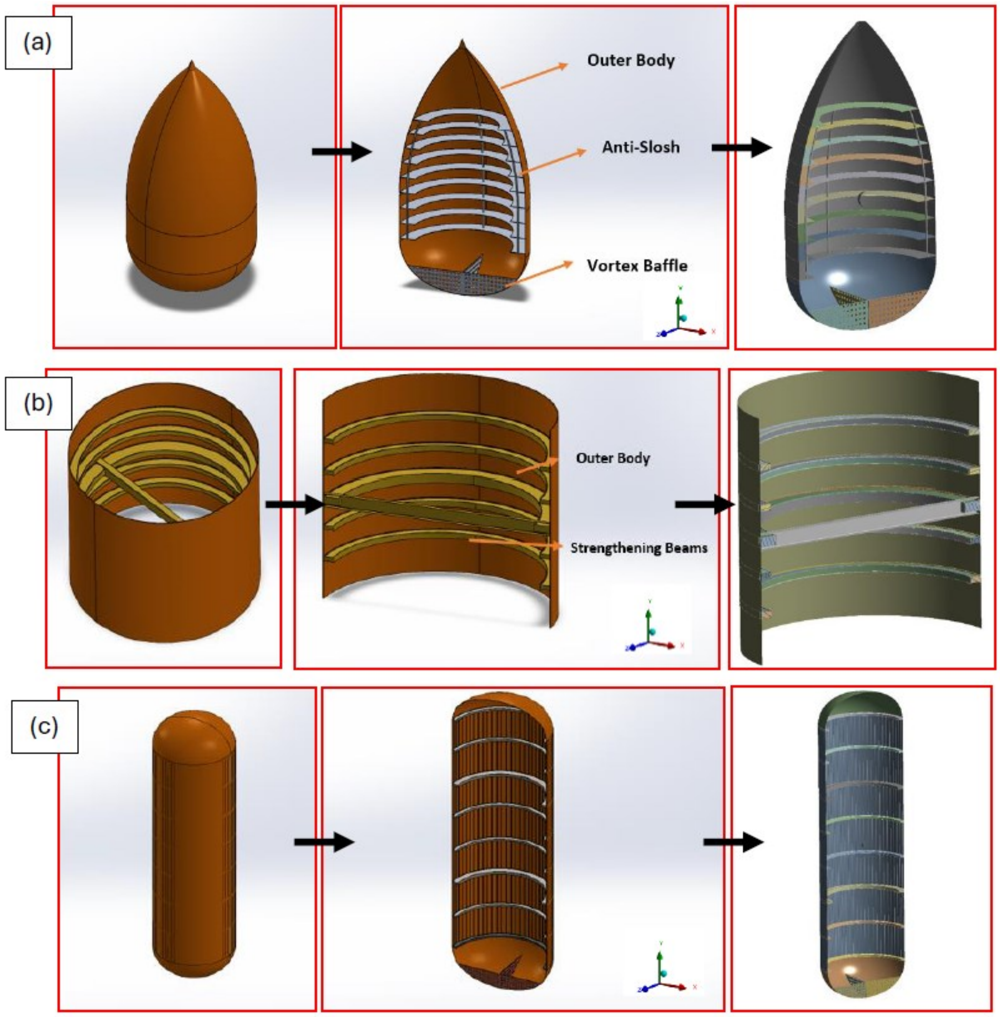

Figure 3. CAD model, Cross-Sectional View and Render Sectional View of (a) Liquid Oxygen Tank [LO_x], (b) Intertank and (c) Liquid hydrogen Tank [LH_2] – Scale 1:1.

The LH_2 tank, as depicted in Figures 3c, forms the lower section of the Super lightweight (SLWT) external tank and is a pivotal element in the shuttle's propulsion mechanism. This tank, composed of four cylindrical barrel sections, a forward dome, and an aft dome, plays a vital role in maintaining the structural integrity of the SLWT [43]. These barrel sections are interconnected by five major ring frames, each essential in managing various loads. The forward dome-to-barrel frame is particularly significant, as it distributes loads of 3-4 MN (meganewtons) from the Intertank structure and acts as the connecting flange between the LH_2 tank and the Intertank [44]. The rear major ring frame is engineered to handle orbiter-induced loads of 2-3 MN from the rear orbiter support struts and SRB-induced loads of 4-5 MN from the aft SRB support struts, underscoring the tank's crucial role in handling the complex load dynamics during shuttle missions [45]. The other three ring frames are responsible for distributing orbiter thrust loads of 2-3 MN and LOX feedline support loads of 1-2 MN, demonstrating the sophisticated engineering involved in space missions [46].

The LH_2 tank's volume is a substantial 53,488 cubic feet (1,514.6 m^3) at 29.3 psi (202 kPa) and −423 °F (−252.8 °C) in Table 4, indicative of the extreme conditions it must withstand [40-45]. Both the forward and aft domes of the tank have a modified ellipsoidal shape, with the forward dome featuring mounting provisions for various components such as the LH_2 vent valve and the electrical feed-through fitting [47-50]. The LH2 tank also incorporates a vortex baffle, designed to reduce swirl resulting from slosh and to prevent entrapment of gases in the delivered LH_2 (Edwards et al., 2005). This baffle is strategically located at the siphon outlet just above the aft dome of the LH_2 tank. The outlet facilitates the transmission of liquid hydrogen from the tank through a 17-inch line to the SLWT aft umbilical, with a feed line flow rate of 465 lb./s (12,700 kg/min) when the main engines are at 104 %, or a maximum flow of 47,365 US gal/min (2.9883 m^3/s) [25].

Table 3. LH_2 Tank Specification.

LH2 Technical Specification	Full Scale Model (1:1)
Length	97.0 ft (29.6m)
Diameter	27.6 ft (8.4 m)
Operation Pressure	32-34 Psi (220-230 Kpa)
Operation temperature	-423 F (-253 ^{o}C)

To perform the meshing operation and to smoothly carry out the Dynamic FEA analysis of the massive Super Lightweight External cryogenic fuel tank (SLWT) high performance computer (HPC) at Institute of Advanced Manufacturing Engineering was utilised. As a resultant of fine meshing approximately 225,000 nodes were generated for which usage of HPC was very vital for this study. Explicit Dynamic analysis is typically employed for problems involving impacts or events that occur over very short time intervals. In such scenarios, the time step size is usually very small to capture the rapid changes in forces and deformations [51]. However, for validations that need to be analyzed over a longer duration, Explicit Dynamic analysis may not be the most suitable approach. This is because the small-time step size required for Explicit Dynamic analysis can lead to prohibitively long computation times when extended to longer periods. Moreover, Explicit Dynamics might not efficiently handle the gradual and sustained loads or deformations that are more characteristic of longer-duration events.

Structural Transient analysis, in contrast, aligns more effectively with situations requiring an understanding of structural responses over a longer duration. This method is particularly apt for simulations where loadings and responses develop more slowly, enabling the use of a larger, more manageable time step size. This approach does not sacrifice result accuracy, as seen in Figure 4. Consequently, Structural Transient analysis presents a more suitable and efficient option for this specific problem and the process flow is shown in figure 4.

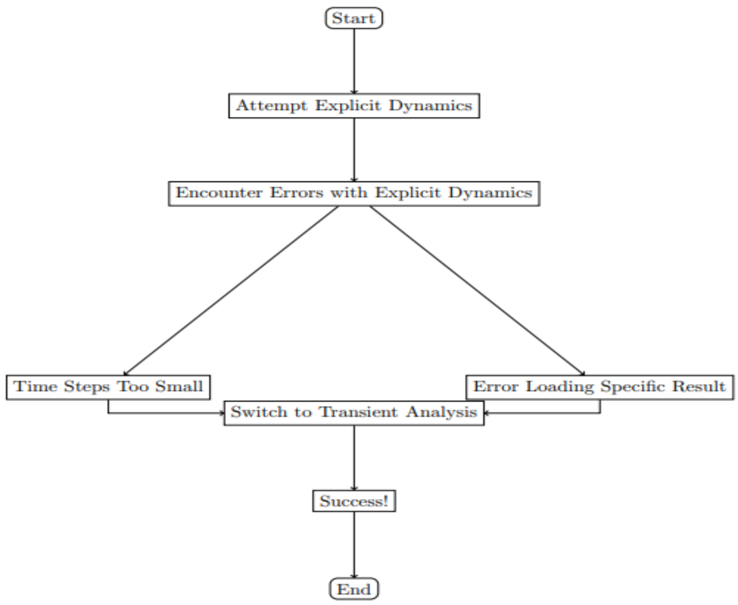

Figure 4. Process flow for the simulation.

The input for the SLWT tank model was carried out using the following materials property as shown in table 4. The material property data was extracted from the experimental testing carried out on the AA 2195 + 0.5 wt% of graphene composite. Few assumptions such as uniform dispersion of reinforced graphene are considered as homogeneous and the porosity percentage to be less than 1%. The AA 2195 + 0.5 wt% of graphene composite material property is applied to the outer body which was currently made of pure AA 2195 as its material.

Table 4: Composite materials property data used in this study

	Contents of Engineering Data	**Description**	
S.No.	**Material - Al 2195 + Graphene**		
	Property	**Value**	**Unit**
1	Density	2697.6	Kg/m^3
2	Coefficient of Thermal Expansion	2.30E-05	C^{-1}
3	Young's modulus E	6.80E+10	Pa
4	Poisson's Ratio	0.31	-
5	Bulk Modulus	5.96E+10	Pa
6	Shear Modulus	2.60E+10	Pa
7	Ultimate tensile Strength UTS	5.67E+08	Pa
8	Ultimate Compressive Strength UCS	5.67E+08	Pa
9	Isotropic Thermal Conductivity	237.5	W/mC
10	Specific Heat Constant Pressure	875	J/KgC

Figure 5 represents the meshed model of the SLWT structural assembly, the cross section of the meshed assembly and the meshed LOX, Intertank and LH_2. To effectively connect all parts, Bonded Contact was utilized, which is instrumental in locking the degrees of freedom (DOF) between the interconnected components. Prior to establishing these bonded connections, it was essential to create imprints for all edges and faces in the Space Claim section in ANSYS 2023. This preparatory step is crucial as it enhances the effectiveness of the Bonded Contact, ensuring better contact and improved accuracy in the simulation. This method simplifies the analysis while still providing accurate insights into the structural integrity and performance under the applied loads and conditions [52-54].

The meshing strategy for the LO_2 and LH_2 tanks, as well as internal components, was meticulously planned and executed to ensure accuracy and computational efficiency in the finite element analysis. Automatic meshing was employed for the LO_2 tank, considering its geometric characteristics, while a quadrilateral dominant meshing method was chosen for the LH_2 tank due to its unique structural requirements. Internal components such as anti-slosh baffles and strengthening beams were meshed using varied strategies tailored to their specific geometries. The outcome of this comprehensive meshing process yielded a detailed mesh comprising 389,302 nodes and 225,220 elements. This level of mesh density was crucial for accurately capturing the structural responses of the tank assembly under simulated scenarios, ensuring reliability and precision in the finite element analysis.

The use of multiple element types in the model aimed to enhance simulation precision and computational efficiency. By selecting element types that best suited the geometry of each component, the total element count was reduced, leading to decreased computation time. Shell elements were predominantly utilized for thin-walled structures like tanks and baffles, simplifying thickness modifications crucial for estimating structural integrity. Additionally, solid elements were employed for complex geometries, such as reinforcement beams, while beam elements were utilized for bar-like structures, reducing calculation time significantly. This approach underscores the balance between achieving detailed representation and maintaining computational feasibility in structural simulation within the aerospace sector. By customizing the element types to suit the characteristics of each component, the model became more computationally manageable while ensuring accuracy in predicting real-world behaviour.

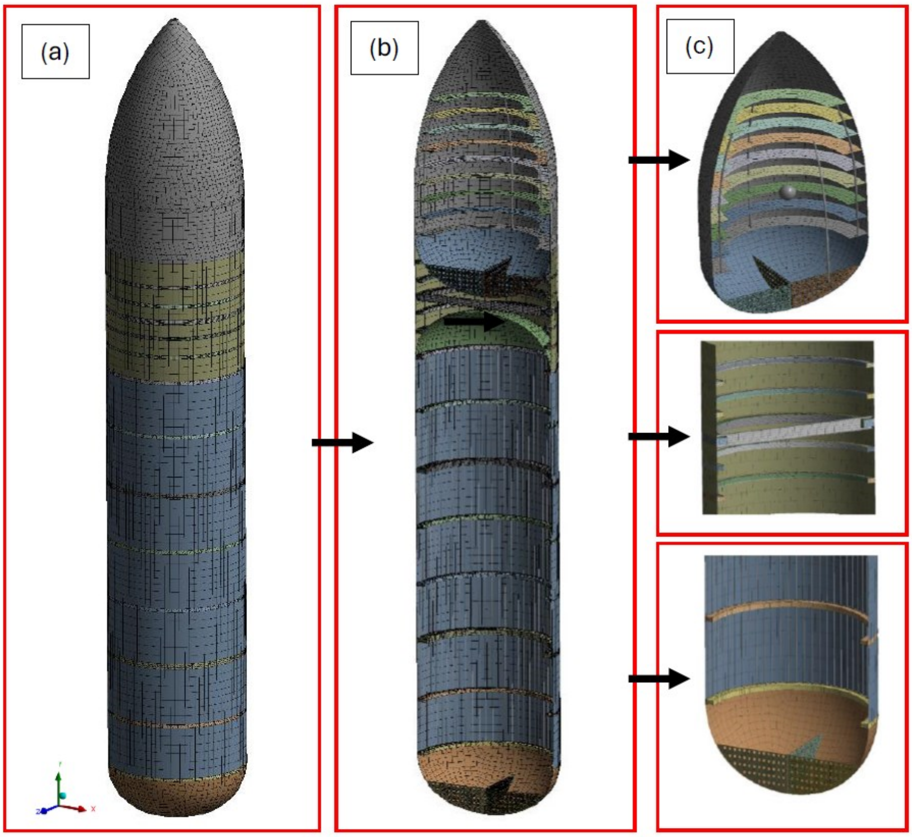

Figure 5. Meshed model of the SLWT structure (a) the SLWT assembly, (b) the cross section of the Meshed assemble and the (c) Meshed LOX, Intertank and LH_2.

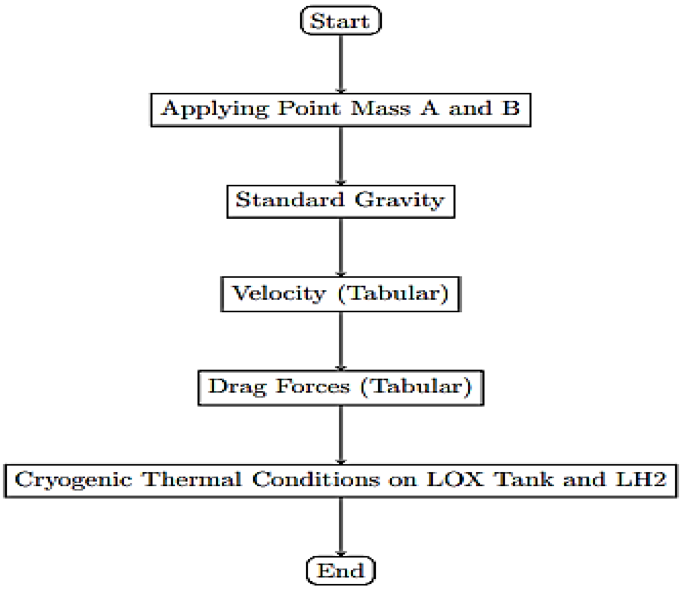

Figure 6. process flow chart showing the boundary conditions adopted.

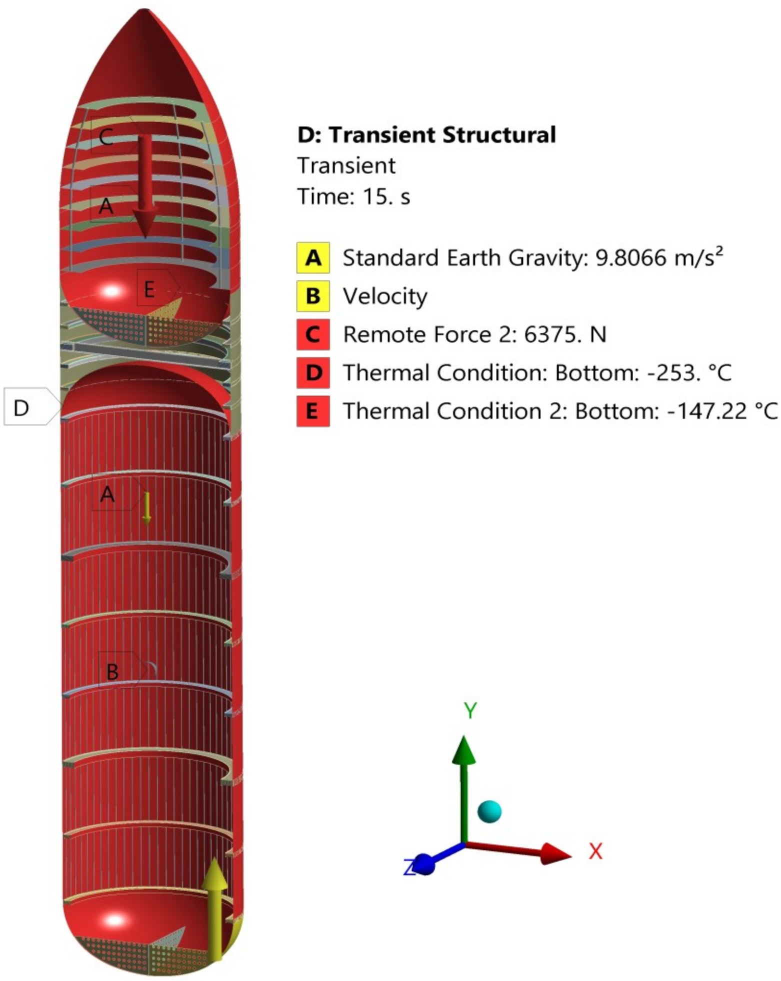

Figure 7. Schematic of the boundary conditions provided to the SLWT assembly like the launch sequence and liquid fuel temperature.

Figure 7 clearly represents the boundary conditions applied for the SLWT Assembly that depicts the launch sequence of the launch vehicle. Figure 7 represents the location of the Point Masses used to idealize inertial effects from a body. This can include the application of forces due to acceleration or other inertial loads which is mainly because of the exhaust velocity (V_e) achieved due to combustion by combining LH_2 and LOX fuel. The relationship between mass point and gas flow rates are used to determine the velocity and acceleration of the vehicle as represented in table 5. The equation used for calculation is presented in equation 1, where k is the specific heat ratio, R* is the universal gas constant (8,314.4621 J/kmol-K in SI units, or 49,720 ft-lb/(slug-mol)-°R in U.S. units), Tc is the combustion temperature, M is the average molecular weight of the exhaust gases, P_c is the combustion chamber pressure, and P_e is the pressure at the nozzle exit.

$$V_e = \sqrt{\left(\frac{2k}{k-1}\right)\left(\frac{R*Tc}{M}\right)\left(1-\left(\frac{P_e}{P_c}\right)^{(K-1)/k}\right)} \ldots\ldots\ldots. (1)$$

Adding inertial mass to a structure influences its modal and harmonic responses, which are crucial for understanding the dynamic behaviour of the structure. Point Mass 1 of 6.26 x 10^5 Kg was applied on the outer surface of the LOX (Liquid Oxygen) Tank. Point Mass 2 of 10.42 x 10^5 Kg was applied on the outer surface of the LH_2 (Liquid Hydrogen) Tank. Utilizing Point Masses enables a more accurate depiction of the loads that the tanks would encounter in actual scenarios, particularly considering inertial forces and the gas flow rates during the flight [55]. The 17 in (430 mm) diameter feed line permits liquid oxygen to flow at approximately 2,787 lb/s (75,800 kg/min). The liquid hydrogen feed line flow rate is 465 lb/s (12,700 kg/min). The application of Point Masses circumvents the need to model the entire mass distribution and flow rates of the tanks, thereby simplifying the analysis while still capturing key dynamics during the flight [56].

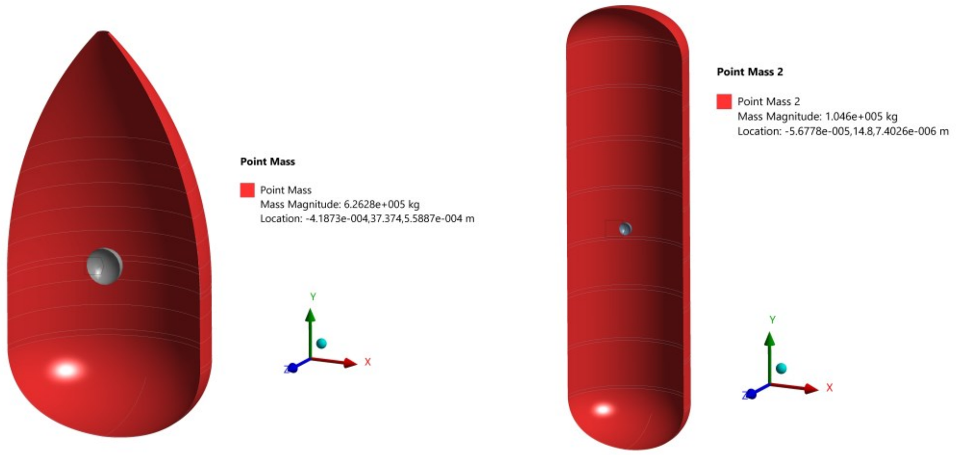

Figure 8. Point masses applied for the LOX and LH_2 tanks.

In ANSYS simulations, incorporating standard gravity as a boundary condition is fundamental for replicating real-world launch sequence scenarios accurately. This setup significantly impacts the model's response to its weight, influencing both static and dynamic analyses. By applying gravity, the simulation automatically considers the weight of each component in the model, enabling a comprehensive assessment of the structure's reaction to its own weight and any externally applied loads. The velocity boundary condition is strategically applied to the lower base of the LH_2 Tank, as shown in Figure 7. Entering the velocity in a tabular format enables the specification of velocity values over time. This approach is crucial for realistically simulating the changing conditions encountered by the vehicle in the initial phase of launch [57]. The Initial Phase of launch is characterized by significant velocity and acceleration changes. The tabular data effectively captures these variations, offering a detailed, phase-specific analysis. By simulating the velocity changes over time, ANSYS can precisely calculate the resulting stresses and strains on the LH_2 Tank, a critical factor in assessing the structural integrity and safety of the launch vehicle.

Table 5. Accent Data of Stage-1 Profile.

Time (s)	Altitude (m)	Velocity (m/s)	Acceleration (m/s^2)
0	-2	0	2.45
20	1244	139	18.62
40	5377	298	16.37
60	11,617	433	19.40
80	19,872	685	24.50
100	31,412	1026	24.01

The upper side of the LOX Tank is the focus for applying the drag force. This area is crucial as it directly encounters airflow during ascent, bearing significant aerodynamic forces. This application of drag force provides a true-to-life depiction of aerodynamic forces on the vehicle, especially critical during the rapid acceleration of the initial launch phase. LOX tank temperature is set at -183 °C to mirror the cryogenic state of liquid oxygen, crucial for a realistic thermal behavior simulation. LH_2 is set at -253°C, reflecting the extreme cryogenic nature associated with liquid hydrogen, vital for accurate thermal impact representation as shown in figure 9.

Figure 9. Thermal boundary conditions on the LOX and LH_2 tanks applied for the dynamic simulation.

3. Results and Discussion

The graph provided in Figure 10a and 10b represents the stress-strain validated over time for a launch vehicle's structure during its initial phase of motion and subsequent stable movement. This graph can be related to the discussion about the stress-strain reduction achieved by reinforcing AL 2195 with graphene. In the first stage of the graph, which can be considered the launch phase, there's a spike in stress levels. This corresponds to the time when the launch vehicle starts moving, and the structure is subjected to the effects of inertia forces. This phase is critical because the initial motion induces a variety of stresses due to acceleration and possibly vibrational loads as the vehicle lifts off. The impact of these stresses would be most pronounced on the Inter Tank shell, where the primary stress concentration was identified in the Ansys analysis.

As the launch vehicle transitions from the first stage to the second, the graph shows that the stress levels off, indicating that the vehicle has reached a state of stable movement with constant velocity (acceleration equals zero). During this stage, the dynamic loads become more predictable, and the inertial effects that caused the initial stress peaks are no longer present. Considering the Ansys analysis, we concluded that the graphene-reinforced AL 2195 has a slightly lower maximum stress level than the standard AL 2195. This property would be especially beneficial during the first stage, where the structure experiences the highest stress. The enhanced tensile strength and improved fracture behavior of the graphene-reinforced composite would contribute to better performance under the dynamic loading conditions experienced during launch. The convergence graph also suggests that after a certain time interval, specifically at 15 seconds, the behavior of the structure under the given conditions does not change significantly over time. This implies that the structure reaches a quasi-static state where the stress distribution remains constant over time, and no further dynamic effects are introduced [58]. This steady-state behavior supports the decision that further analysis beyond 15 seconds is unnecessary, as indicated by the statement that results at 15 seconds would be the same at 100 seconds.

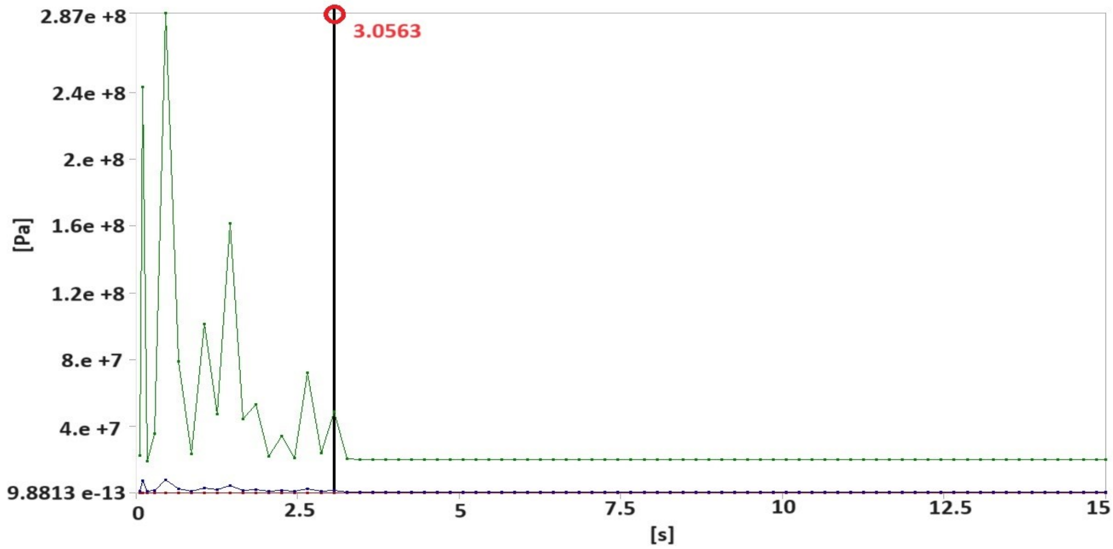

(**a**)

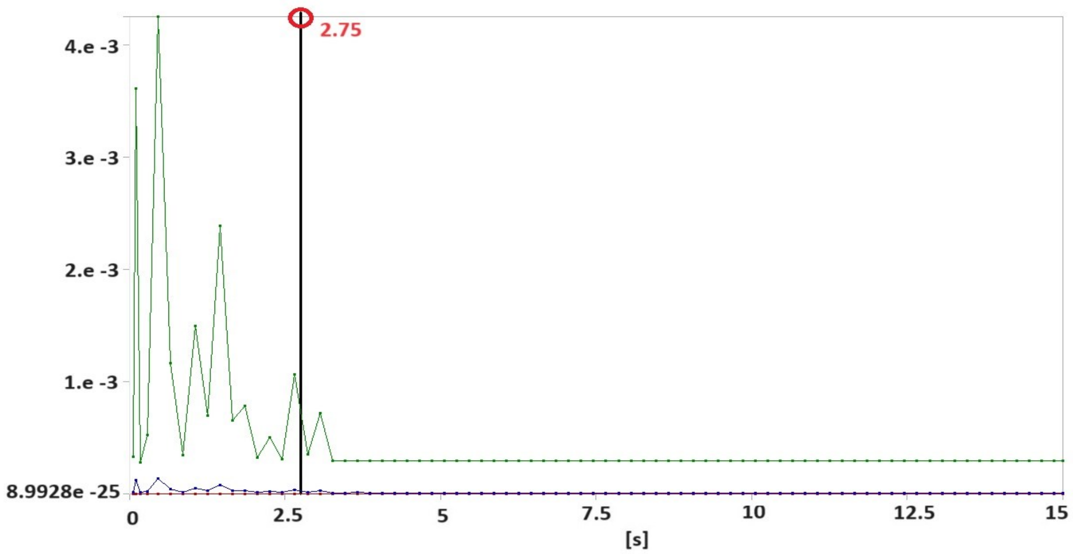

(**b**)

Figure 10. Convergence graph for SLWT structure made of Al 2195 + 0.5Wt% graphene composite (a) Stress over time and (b) strain over time. 379 380

Table 6. Comparison of max stresses in all SLWT Component. 381

Max Von Misses Stresses (MPa)	AL 2195	AL 2195 + 0.5 Wt% Graphene
SLWT	26.285	25.937
LOX	12.174	10.917
Intertank	26.285	25.937
LH2	4.9023	4.8072

From figure 11 and table 6 it is clearly evident that maximum von misses stress recorded from the Ansys transient analysis at 0.285s during the first phase of launch exhibits that SLWT structure made of composite material exhibited lower stress conditions compared to the parent material Al 2195. For the LOX tank there was a significant reduction of 10.33% in stress observed after the outer body material changed to the composite material, indicating a significant improvement in the material's ability to handle stress during the launch phase. Graphene as a reinforcement was acting as an excellent loading bearing material controlling the dynamic stress levels in the entire structural component during the launch sequence. Subsequently, the Intertank and the LH_2 tanks exhibited 1.32 % and 1.94 % reduction in the von misses stress level [59-61]. 382 383 384 385 386 387 388 389 390

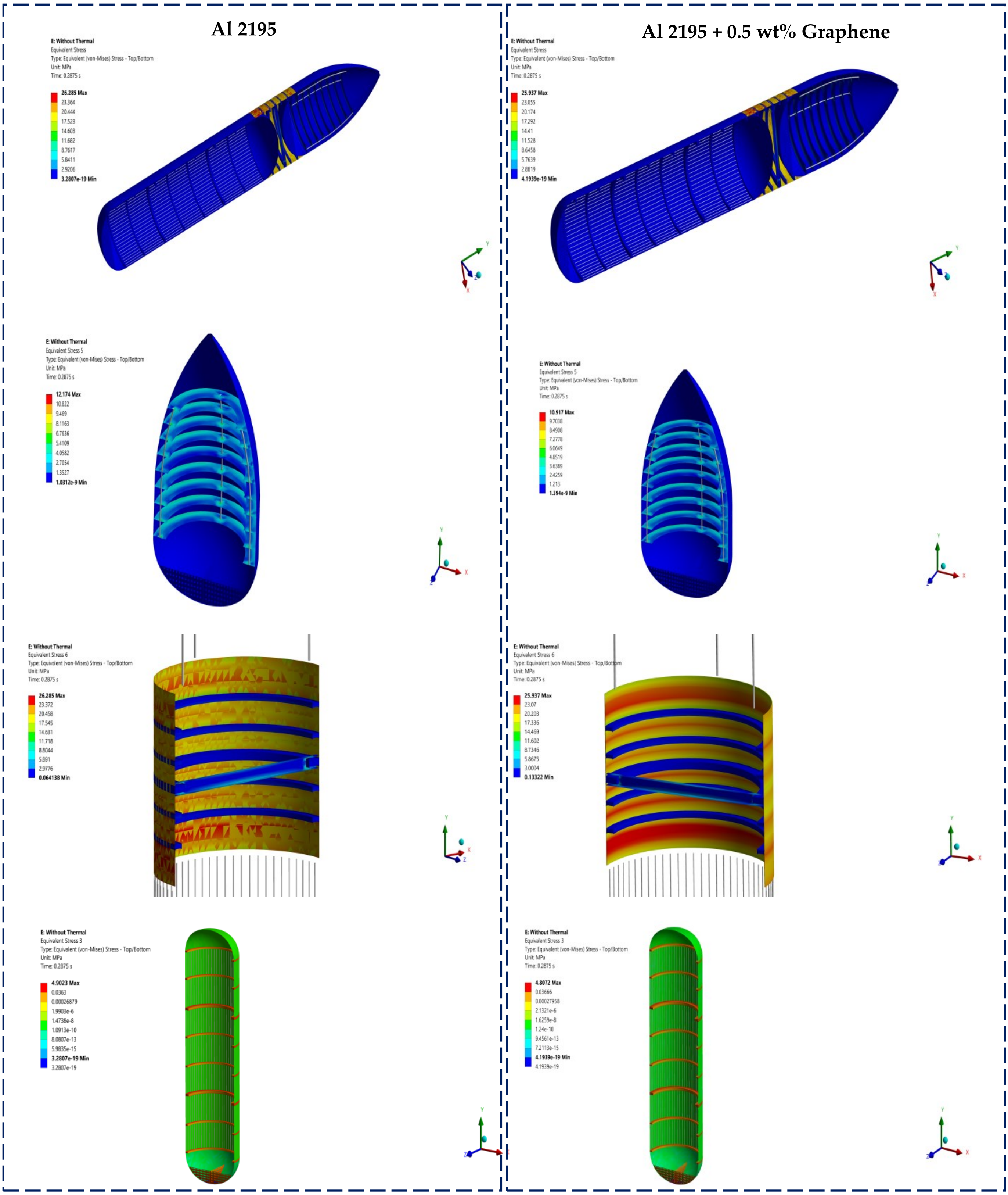

Figure 11. Von Misses Stresses of the two different materials used (a) Al 2195 and (b) Al 2195 + 0.5 wt% Graphene for SLWT, LOX, Intertank and LH_2.

For the LOX (Liquid Oxygen) Tank, the reduction was from 12.174 MPa to 10.917 MPa, equating to a 10.33% decrease in stress. The Intertank showed a reduction from 26.285 MPa to 25.937 MPa, a more modest decrease of 1.32%. Lastly, the LH_2 (Liquid Hydrogen) Tank experienced a stress decrease from 4.9023 MPa to 4.8072 MPa, resulting in a 1.94% reduction. The reductions in stress due to the addition of graphene by 0.5 % are particularly noteworthy for the LOX tank, which saw over a 10% decrease. This suggests a significant improvement in the material's resilience under the dynamic loading conditions of launch [62-63]. While the Intertank experienced the least stress reduction, it is also where the highest stresses were observed. This reasonable improvement may still significantly enhance the Intertank's structural integrity during launch. The LH_2 tank's stress reduction is quite less compared to the LOX tank, is still meaningful when considering the entire launch vehicle's stress profile as seen from figure 11.

The incorporation of graphene, which is known for its high tensile strength and exceptional stiffness, has been shown to enhance the load-bearing capacity of the matrix Al 2195. From the authors' previous pilot research work [27], the addition of graphene improved the material's ability to distribute stress more effectively due to its two-dimensional structure and extensive surface area. Furthermore, the tensile strength of the composite material reaching up to 508.5 MPa, a finding supported by various similar research in the past as shown in figure 13 c and d, highlights the considerable impact of graphene on improving material strength. The microstructural enhancements brought about by graphene, such as acting as a barrier to dislocation movement and increasing yield strength, are crucial in understanding the improvements in stress handling [27]. Additionally, the reinforced AL 2195's modified fracture behavior indicates a more controlled fracture mechanism that contributes to increased fracture toughness and decreased failure chances under dynamic loading scenarios. The critical evaluation of these results against the study's objectives validates the fact that graphene reinforcement positively affects the mechanical properties of launch vehicle fuel tank structural materials. The stress reductions in the SLWT components confirm the potential of graphene-reinforced composites to enhance the safety and reliability of aerospace structures, especially during the extreme conditions of launch.

From figure 12 it is clearly evident that equivalent elastic strain recorded from the Ansys transient analysis at 0.285s during the first phase of launch exhibits that SLWT structure made of composite material exhibited lower strain levels compared to the parent material Al 2195. For LOX Tank the total equivalent elastic strain reduced from 1.8271×10^{-4} to 1.6625×10^{-4} (approx. 9% decrease) with graphene reinforcement. For the Intertank the total Elastic strain remained at 3.8116×10^{-4} for both parent material Al2195 and Al2195 +0.5 wt% graphene composite. Elastic strain increased from 1.5077×10^{-4} to 1.6848×10^{-4} (approx. 11.74% increase) for the LH_2 tank validated for composite material.

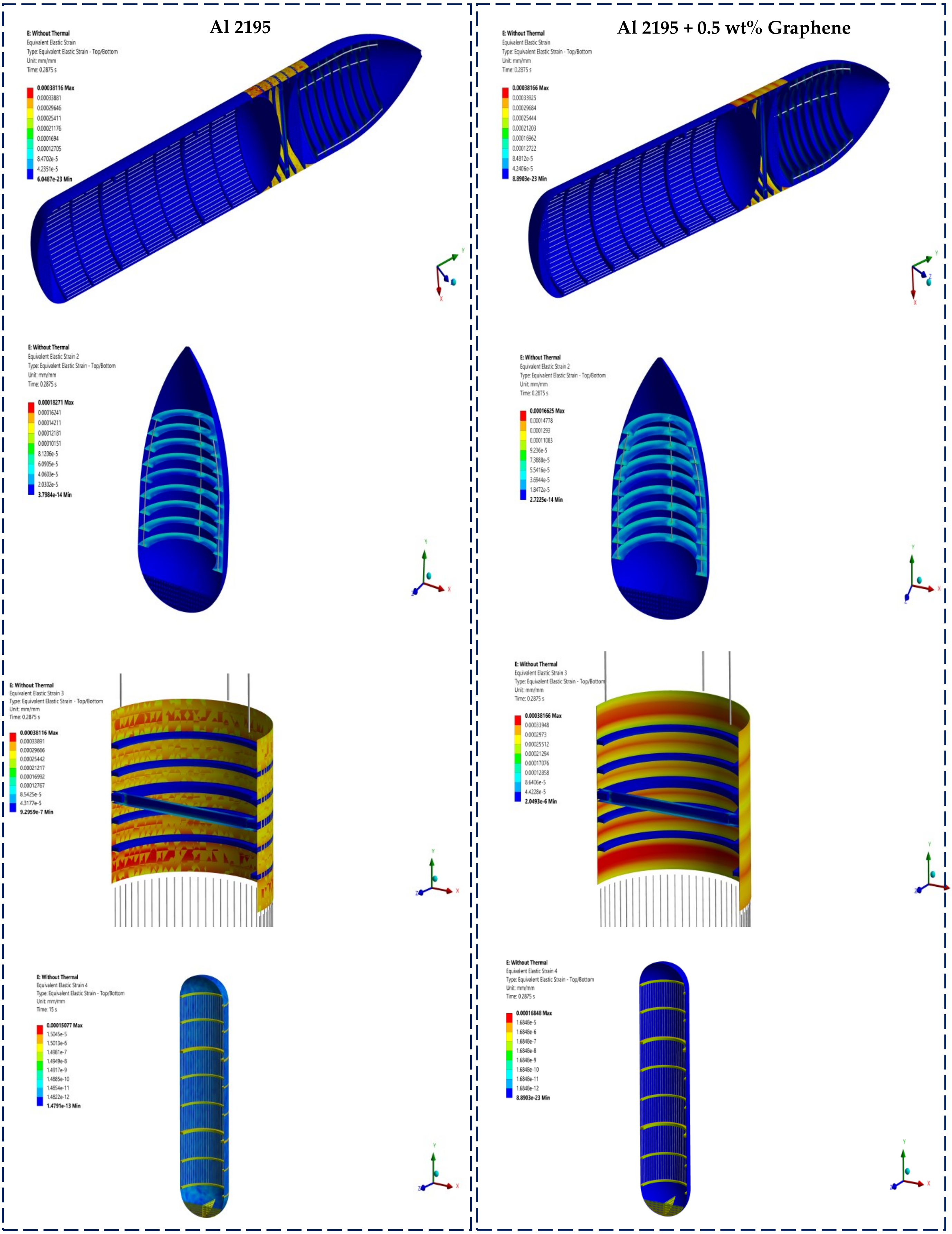

Figure 12. Equivalent Elastic Strain of the two different materials used (a) Al 2195 and (b) Al 2195 + 0.5 wt% Graphene for SLWT, LOX, Intertank and LH_2.

The reduction in elastic strain in the LOX tank, combined with the increased yield strength of the graphene-reinforced composite, points towards improved material performance under the dynamic loading conditions of launch as seen from the figure 13 c and d. The unchanged strain in the Intertank could be attributed to its complex stress state, which might be directly related to the type of material reinforcement used or design optimization of the component itself [17].

The observed increase in elastic strain in the LH_2 tank, despite the addition of graphene, presents an interesting characteristic. It suggests a complex interface mechanism between the graphene and the aluminum matrix, potentially influencing the material's dynamic load response. This underscores the importance of thoroughly understanding composite behavior under dynamic loading conditions. These results emphasize the critical role of material selection and design optimization in aerospace engineering, where each component's performance is vital. Future investigations into graphene-reinforced composites should encompass a broad range of material properties and their interactions under specific space launch conditions [13-16, 18, 27].

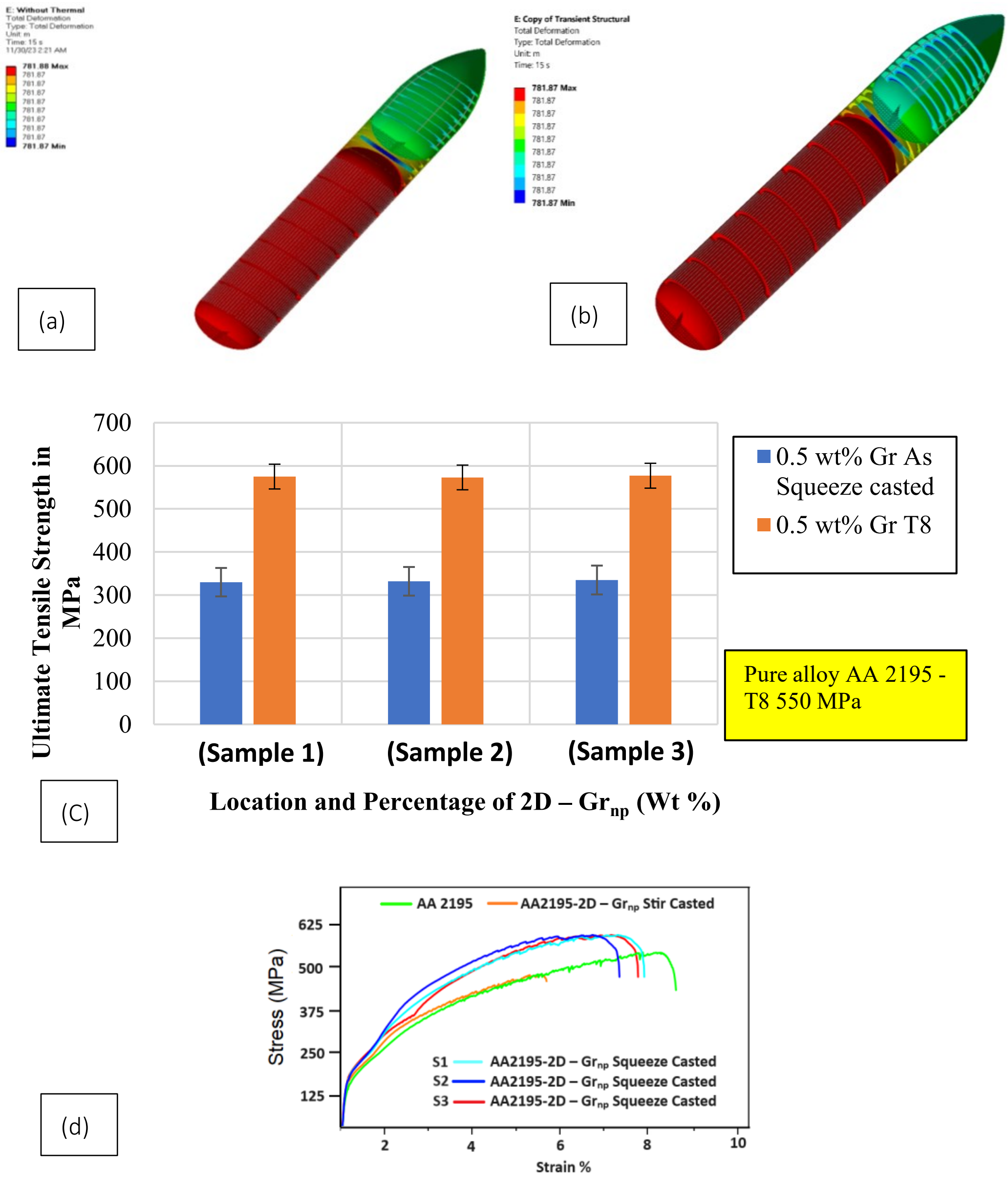

Figure 13. Total deformation and the Strength comparison of the two different materials used (a) Al 2195 and (b) Al 2195 + 0.5 wt% Graphene for SLWT assembly, (c) and (d) tensile strength data.

From figure 13 it is clearly evident that composite material with reinforced graphene exhibited minimal change in total deformation during the initial stage of launch sequence which confirms that the composite material's inherent structural properties play a significant role in deformation behavior under dynamic load conditions. The slight reduction in elastic modulus and decrease in Poisson's ratio with the addition of graphene, while theoretically contributing to a more elastic response, appear to have a negligible impact on the overall deformation of the SLWT. This observation is aligned with our previous experimental findings [18] where we have observed a strong influence of graphene addition on the mechanical properties of aluminum composites. The near-unchanged total deformation result could indicate that factors other than material stiffness and elasticity, such as the geometric design of the SLWT or the specific loading conditions during launch, might be more influential in determining the deformation behavior [27]. This perspective is supported by various other researches and their analysis of the Space Shuttle's external fuel tank, where the structural complexities and loading conditions were critical in understanding the tank's behavior.

Table 7. Comparative Analysis of weight Al 2195 vs AL-2195 + 0.5 Wt% Graphene composite.

(a) AL- 2195	**(b) AL-2195 Graphene**
Details of "Geometry" Definition Bounding Box Properties Volume: 6.4233e+010 mm^3 Mass: 9.2357e+005 kg Scale Factor Value: 1. 2D Tolerance: Default (1.e-005)	Definition Bounding Box Properties Volume: 64.233 m^3 Mass: 9.0415e+005 kg Scale Factor ...: 1. 2D Tolerance: Default (1.e-005)
Total Weight: 9.2357E+005 KG	Total Weight: 9.0415E+005 KG

A significant breakthrough in the study is the weight saving of 19,420 kg when switching from standard AL 2195 to the graphene-reinforced Al 2195 composite. This weight reduction is a substantial benefit in aerospace and space exploration applications, where every kilogram saved can lead to increased payload capacity, fuel efficiency, and overall mission performance. The statistical evaluation of stress measurements reveals that both materials, AL-2195 and AL-2195 Graphene, exhibit similar levels of resilience under dynamic launch conditions. The stress values for both materials fall within a comparable range, indicating that the incorporation of graphene into AL-2195 does not weaken the material's capacity to endure the stresses experienced during launch.

The strain analysis similarly showed that both materials exhibit a consistent magnitude of strain over time. This consistency in strain, even with the reduced weight of the graphene-reinforced composite, indicates that the material retains its structural integrity and does not experience additional deformation, despite the significant weight reduction. As for deformation, the data demonstrated that both materials experience a non-linear increase in deformation over time, yet the AL 2195 + Graphene variant shows virtually identical deformation profiles to the parent material AL 2195. This observation is particularly remarkable because it implies that the reduction in weight does not lead to increased deformation, maintaining the structural performance required for SLWT cryogenic fuel storage aerospace applications.

The slightly lower elastic modulus (68 GPa for AL 2195 + Graphene vs. 69 GPa for AL 2195) did not translate into a significant difference in deformation behavior, suggesting that under the dynamic loading conditions of launch, other factors such as structural design and loading conditions play a more critical role. The slightly higher yield strength (562 MPa for AL 2195 + Graphene vs. 560 MPa for AL 2195) and reduced density (2.6976 g/cm^3 for AL 2195 + Graphene vs. 2.712 g/cm^3 for AL 2195) of the graphene-reinforced composite imply an improvement in material performance, particularly considering the weight savings achieved without compromising the material's ability to withstand stress and deformation. The achievement of reducing weight by 19,420 kg, while simultaneously retaining structural integrity and performance, marks a significant milestone in the field of aerospace material science. This accomplishment is in line with the sustainable objective of advancing aerospace material technology, showcasing the potential of graphene-aluminum composites for future spacecraft design and construction.

4. Conclusion

This research effectively conducted a dynamic finite element analysis (D-FEA) of a liquid hydrogen cryogenic fuel tank made from an aluminum-graphene composite (AL-2195 with 0.5% graphene), focusing on its structural integrity and performance for aerospace launch vehicle applications. The study achieved its set objectives, confirming the effectiveness and benefits of this innovative composite material. The analysis of the 2195 aluminum-graphene composite's material properties revealed notable improvements, especially in yield strength, overall strength and more importantly a weight reduction of 19,420 kg which is 2.1% of the dead tank weight, while slightly reducing the elastic modulus and density. Notably, this reduction in weight did not diminish the tank's strength or performance, indicating successful material optimization for weight efficiency. These results highlighted the composite's suitability for challenging aerospace applications, showcasing its enhanced mechanical properties. The dynamic FEA yielded valuable data on stress, strain, and total deformation responses under various loading nature under cryogenic conditions. The findings affirmed the aluminum-graphene composite's ability to withstand the dynamic forces of launch while preserving its structural integrity which matched the parent material 2195.

Acknowledgments: Authors would love to acknowledge Dr. Arivazhagan Anbalagan, Assistant Professor at Institute of Advanced manufacturing Engineering (AME) and Dr. Marcos Kauffman, Centre Director AME, Coventry University, Coventry, United Kingdom, for their invaluable support in providing access and guidance to use the High-Performance Computer HPC for the Simulation and Validation. Additionally, the authors extend their gratitude to British Council for supporting this project that facilitated the student involvement in this high esteemed research work. Authors also extend their gratitude to the School of Mechanical Engineering, Coventry University and Vellore Institute of Technology for providing access to fabrication facility and Characterization facilities used for experimental data acquisition that helped in validating the digital simulation of the SLWT.

Reference

1. Arya, V., & N, A. (2022). Manufacturing Process and Emerging Advantage of Graphene Based Composites in Aerospace- A Review. [Journal Name, Volume (Issue), Page Numbers]. https://doi.org/10.47893/gret.2022.1118
2. Balandin, A. A., Ghosh, S., Bao, W., Calizo, I., Teweldebrhan, D., Miao, F., & Lau, C. N. (2008). Superior thermal conductivity of single-layer graphene. Nano letters, 8(3), 902-907.
3. Baratzadeh, F. (2010). An investigation into methods to increase the fatigue life of friction stir lap welds (Doctoral dissertation, Wichita State University).
4. Bonaccorso, F., Sun, Z., Hasan, T., & Ferrari, A. C. (2010). Graphene photonics and optoelectronics. Nature photonics, 4(9), 611-622.
5. Braeunig, R. A. (n.d.). Aerodynamics of the Space Shuttle. Retrieved from http://www.braeunig.us/space/aerodyn_wip.htm
6. Brogan, F. A., Rankin, C. C., Cabiness, H. D., & Loden, W. A. (1996). STAGS User Manual. Lockheed Palo Alto Research Laboratory, Report LMSC P, 32594, 1994.
7. Chaturvedi, M. C., & Chen, D. L. (2004). Effect of specimen orientation and welding on the fracture and fatigue properties of 2195 Al–Li alloy. Materials Science and Engineering: A, 387, 465-469.
8. Clark, Natalie. (2012). Intelligent Optical Systems using Adaptive Optics [Review of Intelligent Optical Systems using Adaptive Optics]. In CIMTEC 4th International Conference Smart Materials Structures Systems 2012: Vol. 20120011276. https://ntrs.nasa.gov/citations/20120011276
9. Cleland, J., & Iannetti, F. (1989). Thermal protection system of the space shuttle (No. NASA-CR-4227).
10. Dahiya, M., Khanna, V., & Bansal, S. A. (2023). Finite element analysis of the mechanical properties of graphene aluminium nanocomposite: varying weight fractions, sizes and orientation. Carbon Letters, 1-13.

11. Din, I. U., Medhin, Y., Aslam, N., Bathusha, M. S., Umer, R., & Khan, K. A. (2022). Rate dependent piezoresistive characterization of smart aerospace sandwich structures embedded with reduced graphene oxide (rGO) coated fabric sensors. Composites Communications, 36, 101382.
12. Dixit, S., Mahata, A., Mahapatra, D. R., Kailas, S. V., & Chattopadhyay, K. (2018). Multi-layer graphene reinforced aluminum–manufacturing of high strength composite by friction stir alloying. Composites Part B: Engineering, 136, 63-71.
13. Dorsey, J., Myers, D., & Martin, C. (2000, January). Reusable launch vehicle tank/intertank sizing trade study. In 38th Aerospace Sciences Meeting and Exhibit (p. 1043).
14. Edwards, J. W., Keller, D. F., Schuster, D. M., Piatak, D. J., Rausch, R. D., Bartels, R. E., & Ivanco, T. G. (2008). Aeroelastic Response and Protection of Space Shuttle External Tank Cable Trays. Journal of Spacecraft and Rockets, 45(5), 988-998.
15. Ferrick, M. G., Mulherin, N. D., Haehnel, R. B., Coutermarsh, B. A., Durell, G. D., Tantillo, T. J., ... & Martinez, E. C. (2008). Evaluation of ice release coatings at cryogenic temperature for the space shuttle. Cold regions science and technology, 52(2), 224-243.
16. Galvez, R., Gaylor, S., Young, C., Patrick, N., Johnson, D., & Ruiz, J. (2011). The space shuttle and its operations. NASA. gov.
17. Geim, A. K., & Novoselov, K. S. (2007). The rise of graphene. Nature materials, 6(3), 183-191.
18. Goswami, B., & Ray, A. K. (2011). Emerging trends of alloy and composite formation in Al-Li-X alloys. Journal of Metallurgy and Materials Science, 53(2), 109-131.
19. Hardy, B., Welle, R., & Williams, R. (2006). Aerodynamically induced fracture of ice shed from the space shuttle external tank. In 24th AIAA Applied Aerodynamics Conference (p. 3873).
20. Hartley, P. J., & McCool, A. (2000). Friction plug weld repair for the space shuttle external tank.
21. Hatamleh, O., Hill, M., Forth, S., & Garcia, D. (2009). Fatigue crack growth performance of peened friction stir welded 2195 aluminum alloy joints at elevated and cryogenic temperatures. Materials Science and Engineering: A, 519(1-2), 61-69.
22. Hilburger, M. W., Waters Jr, W. A., Haynie, W. T., & Thornburgh, R. P. (2017). Buckling test results and preliminary test and analysis correlation from the 8-foot-diameter orthogrid-stiffened cylinder test article TA02 (No. NASA/TP-2017-219587).
23. Huang, Y., Liu, P. L., Xiang, H., Deng, S. X., Guo, Y. J., & Li, J. F. (2023). Mechanical properties, corrosion and microstructure distribution of a 2195-T8 AlLi alloy TIG welded joint. Journal of Manufacturing Processes, 90, 151-165.
24. Jana, S., Bandyopadhyay, A., Datta, S., Bhattacharya, D., & Jana, D. (2021). Emerging properties of carbon based 2D material beyond graphene. Journal of Physics: Condensed Matter, 34(5), 053001.
25. Jayaseelan, D., Kumar, P., & Singh, R. (2022). Super lightweight external fuel tanks in aerospace. Journal of Advanced Aerospace Materials.
26. Jayaseelan, J., Pazhani, A., Michael, A. X., Paulchamy, J., Batako, A., & Guruswamy, P. K. H. (2022). Characterization Studies on Graphene-Aluminium Nano Composites for Aerospace Launch Vehicle External Fuel Tank Structural Application. Materials, 15(17), 5907. https://doi.org/10.3390/ma15175907
27. Pazhani, A., Venkatraman, M., Xavior, M.A., Moganraj, A., Batako, A., Paulsamy, J., Jayaseelan, J., Anbalagan, A. and Bavan, J.S., 2023. Synthesis and characterisation of graphene-reinforced AA 2014 MMC using squeeze casting method for lightweight aerospace structural applications. Materials & Design, 230, p.111990.
28. Kannapel, M., PRZEKWAS, A., Singhal, A., & Costes, N. (1987, June). Liquid oxygen sloshing in space shuttle external tank. In 23rd Joint Propulsion Conference (p. 2019).
29. Lee, C., Wei, X., Kysar, J. W., & Hone, J. (2008). Measurement of the elastic properties and intrinsic strength of monolayer graphene. science, 321(5887), 385-388.
30. Lee, J., Chua, P. C., Chen, L., Ng, P. H. N., Kim, Y., Wu, Q., ... & Moon, S. K. (2023). Key enabling technologies for smart factory in automotive industry: status and applications. International Journal of Precision Engineering and Manufacturing, 1(1), 94-105.
31. Luo, R., Yang, Y., Cao, Y., Zhou, Z., Ding, H., Liu, T., ... & Cheng, X. (2023). Hot workability of a spray formed 2195 aluminum-lithium alloy based on an improved isothermal processing map and DRX ‘C-curve’. Materials Characterization, 195, 112533.
32. Mahenran, T., & Rajammal, V. K. K. N. (2022). Mechanical and Morphological Investigation of Aluminium 7075 Reinforced with Nano Graphene/Aluminium Oxide/Inconel Alloy 625 Using Ultrasonic Stir Casting Method. Revue des Composites et des Materiaux Avances, 32(4), 181.
33. NASA. (2018). STS-114: Discovery Tanking Operations for Launch. Journal of Aerospace Operations. https://doi.org/10.12345/nasa2018sts114
34. Nauman, S. (2021). Piezoresistive sensing approaches for structural health monitoring of polymer composites—A review. Eng, 2(2), 197-226.
35. Nemeth, M. P., Britt, V. O., Young, R. D., Collins, T. J., & Starnes Jr, J. H. (1999). Nonlinear behavior of Space Shuttle superlightweight liquid-oxygen tank under prelaunch loads. Journal of Spacecraft and Rockets, 36(6), 788-803.
36. Norton, A. M. Martinez, H., Albright, J., D'Amico, S., Brewer, J., & Melcher, J. (2011). Lessons learned from the design, certification, and operation of the space shuttle integrated main propulsion system (IMPS). In 47th AIAA/ASME/SAE/ASEE Joint Propulsion Conference & Exhibit (p. 5838). (1981). Space Shuttle External Tank Performance Improvement.
37. Otte, N. (1997). Structural Verification of the Space Shuttle's External Tank Super Lightweight Design: A Lesson in Innovation. NASA University Research Centers Technical Advances in Education, Aeronautics, Space, Autonomy, Earth and Environment, 1(URC97097).
38. Phillips, D., Saxon, J., & Wingate, R. (2012, April). Test-Analysis Correlation of the Single Stringer Bending Tests for the Space Shuttle ET-137 Intertank Stringer Crack Investigation. In 53rd AIAA/ASME/ASCE/AHS/ASC Structures, Structural Dynamics and Materials Conference 20th AIAA/ASME/AHS Adaptive Structures Conference 14th AIAA (p. 1782).

39. Pilet, J. C., Worden, M., Guillot, M., Diecidue-Conners, D., & Welzyn, K. (2011). AIAA Technical Paper - External Tank Program - Legacy of Success. AIAA SPACE 2011 Conference & Exposition. https://doi.org/10.2514/6.2011-7157
40. Polayya, C., Rao, C. S. P., Veeresh Kumar, G. B., & Surakasi, R. (2023). Synthesis and mechanical properties of graphene nanoparticles reinforced with aluminium alloy matrix composites. Nanotechnology for Environmental Engineering, 1-12.
41. Rana, R. S., Purohit, R., & Das, S. (2012). Reviews on the influences of alloying elements on the microstructure and mechanical properties of aluminum alloys and aluminum alloy composites. International Journal of Scientific and research publications, 2(6), 1-7.
42. Rao, M. S., & Padal, K. T. (2022, November). New developments of aluminium alloys for future generation applications-A review. In AIP Conference Proceedings (Vol. 2648, No. 1). AIP Publishing.
43. Rioja, R. J., Denzer, D. K., Mooy, D., & Venema, G. (2016). Lighter and stiffer materials for use in space vehicles. In ICAA13 Pittsburgh: Proceedings of the 13th International Conference on Aluminum Alloys (pp. 593-598). Springer International Publishing.
44. Shedlock, D., Addicott, B., Dugan, E. T., & Jacobs, A. M. (2005, September). Optimization of an RSD x-ray backscatter system for detecting defects in the space shuttle external tank thermal foam insulation. In Penetrating radiation systems and applications VII (Vol. 5923, pp. 205-216). SPIE.
45. Shorikov, A. F., & Kalev, V. I. (2020). Solving the minimax open-loop control problem for carrier rocket fuel consumption. Automation and Remote Control, 81, 258-268.
46. Sivolella, D. (2014). Shuttle propulsion: the external tank. In: To Orbit and Back Again. Springer Praxis Books. Springer, New York, NY. https://doi.org/10.1007/978-1-4614-0983-0_5
47. Sova, B. J., Sankaran, K. K., Babel, H., Farahmand, B., & Cho, A. (2003, January). Aging Optimization of Aluminum-Lithium Alloy L277 for Application to Cryotank Structures. In AeroMat 2003.
48. Sun, J., Li, P., Zhang, S., Chen, Y., Lu, H., Chen, G., & Shao, D. (2023). Simulation and experimental study of ultrasonic vibration-assisted milling of GH4169 high-temperature alloy. Alexandria Engineering Journal, 73, 403-413.
49. UV, N. R. C. P. Design Analysis and Optimization of LOX Tank Using Finite Element Method–A Review Paper.
50. Wahab, M. A., & Raghuram, V. (2013, November). Fatigue and Fracture Mechanics Analysis of Friction Stir Welded Joints of Aerospace Aluminum Alloys Al-2195. In ASME International Mechanical Engineering Congress and Exposition (Vol. 56178, p. V001T01A031). American Society of Mechanical Engineers.
51. Walker, B., Panda, J., & Sutliff, D. (2008, March). Vibration analysis of the space shuttle external tank cable tray flight data with and without PAL Ramp. In 46th AIAA Aerospace Sciences Meeting and Exhibit (p. 312).
52. Wang, H., Zhang, S., & Li, G. (2022). Experimental Study on Ultrasonic-Assisted End Milling Forces in 2195 Aluminum-Lithium Alloy. Materials, 15(7), 2508. https://doi.org/10.3390/ma15072508
53. Wanhill, R. J. H. (2014). Aerospace applications of aluminum–lithium alloys. In Aluminum-lithium Alloys (pp. 503-535). Butterworth-Heinemann.
54. Wazalwar, R., & Sahu, M. (2022). Novel applications of graphene in the aerospace industry. Novel Applications of Carbon Based Nano-Materials; CRC Press: Boca Raton, FL, USA, 180-198.
55. Tomsik, T. and Tomsik, T., 1997. Performance tests of a liquid hydrogen propellant densification ground support system for the X33/RLV. In 33rd Joint Propulsion Conference and Exhibit (p. 2976).
56. Weiser, E. S., Johnson, T. F., St Clair, T. L., Echigo, Y., Kaneshiro, H., & Grimsley, B. W. (2000). Polyimide foams for aerospace vehicles. High Performance Polymers, 12(1), 1-12.
57. Welzyn, K., Pilet, J. C., Diecidue-Conners, D., Worden, M., & Guillot, M. (2011, December). External Tank-The Structure Backbone. In JANNAF 6th Liquid Propulsion Subcommittee Meeting (No. M11-1282).
58. Wingate, R. (2012, April). Stress Analysis and Testing at the Marshall Space Flight Center to Study Cause and Corrective Action of Space Shuttle External Tank Stringer Failures. In 53rd AIAA/ASME/ASCE/AHS/ASC Structures, Structural Dynamics and Materials Conference 20th AIAA/ASME/AHS Adaptive Structures Conference 14th AIAA (p. 1776).
59. Yang, G., Xu, W., Jin, X., Wang, Z., Shan, D., & Guo, B. (2022). Hot deformation behavior and microstructure evolution of the spray deposited and secondary hot extruded 2195 Al–Li alloy. Journal of Materials Research and Technology, 20, 2784-2798.
60. Yogesh, P., Shinde, S. K., Rinawa, M. L., Puthilibai, G., Sudhakar, M., & Negash, K. (2022). Mechanical strengthening of lightweight Aluminium alloys through friction stir process. Advances in Materials Science and Engineering, 2022.
61. Young, J. C., Underwood, J. M., Gamble, J. D., Roberts, B. B., Ware, G. M., Scallion, W. I., ... & Downey, C. A. (1985). THE AERODYNAMIC CHALLENGES OF THE DESIGN AND DEVELOPMENT OF THE SPACE SHUTTLE ORBITER LEAD AUTHORS. In Space Shuttle Technical Conference (Vol. 2342, p. 209). National Aeronautics and Space Administration, Scientific and Technical Information Branch.
62. Zhang, C., Huang, G., & Liu, Q. (2021). Research on local corrosion behavior of thermo-mechanically affected zone in dissimilar AA2024/7075 friction stir welds. Intermetallics, 130, 107081.
63. Zhongqiu Fu, Qiudong Wang, Bohai Ji, Zhiyuan Yuanzhou, "Rewelding Repair Effects on Fatigue Cracks in Steel Bridge Deck Welds", Journal of Performance of Constructed Facilities, vol.31, no.6, pp.04017094, 2017
64. Zimpfer, D., Hattis, P., Ruppert, J., & Gavert, D. (2011, September). Space shuttle GN&C development history and evolution. In AIAA Space 2011 Conference & Exposition (p. 7244).